Integrating Airborne LiDAR and OpenStreetMap Features for Automated Hydrological Conditioning of Urban Digital Elevation Models

Tommaso Destefanis[1,2,3], Elena Durando[3], Matilde Oliveti[3], Emanuele Artù Cassin[3], Martina Di Rita[1]

[1] Politecnico di Torino, Interuniversity Department of Regional and Urban Studies and Planning (DIST), Turin, Italy
[2] Sapienza University of Rome, Department of Civil, Constructional and Environmental Engineering (DICEA), Rome, Italy
[3] Ithaca S.r.l., Turin, Italy

Keywords: Digital Elevation Model, Hydrological Conditioning, LiDAR, OpenStreetMap, Data Integration

Abstract

High-resolution Digital Elevation Models (DEMs) are essential for urban flood modelling, where small elevation differences govern drainage and inundation extent. However, DEMs frequently contain hydrological inconsistencies: bridges, tunnels and culverts appear as artificial barriers disrupting flow continuity, while flood defence structures may be poorly represented at the available resolution. This paper presents an automated open-source Python pipeline for generating hydrologically conditioned DEMs by integrating classified airborne LiDAR data with OpenStreetMap (OSM) infrastructure features. The workflow is tested on a 16 km² area over Copenhagen city centre using a 2023 national LiDAR acquisition (13.5 pts/m²). A 0.5 m resolution DSM is generated from LiDAR ground and building classes via Inverse Distance Weighting (k=12, power=2, max radius 5 m), with Nearest Neighbour gap-filling. Hydrological conditioning applies four sequential operations: bridge burning at 108 footprints, tunnel enforcing at 53 shallow underpasses, culvert enforcing at 8 subsurface passages, and barrier rasterization raising 199 flood defence structures to their LiDAR-measured top-of-wall elevations. In total, 198,733 pixels were lowered (median 0.69 m) and 27,022 raised (median 3.00 m above ground), reducing the trapped depression volume in the DSM by 718,496 m³ (-5.0%). Vertical accuracy is assessed against the Danish national terrain model DHM/Terræn (NMAD = 0.066 m, LE90 = 0.265 m). The conditioned DEM feeds the CLEAR-EO urban flood simulation chain at the Danish Meteorological Institute; full hydraulic validation is outside the scope of this work. The pipeline is modular and transferable to other urban contexts with pre-classified LiDAR and OSM data.

1. Introduction

Floods are among the most damaging natural hazards globally, and their frequency and intensity are projected to increase under climate change scenarios, particularly in urban areas where progressive impermeabilization intensifies surface runoff and reduces drainage capacity (IPCC, 2022). Copenhagen exemplifies this vulnerability: the July 2011 cloudburst delivered over 100 mm of rainfall in two hours, causing damages exceeding €800 million and prompting the city’s comprehensive Cloudburst Management Plan (City of Copenhagen, 2012; Arnbjerg-Nielsen et al., 2013). In European cities, pluvial flood risk is especially sensitive to small-scale topographic variations: differences of tens of centimetres can determine whether water accumulates, drains or routes towards critical infrastructure. Digital Elevation Models (DEMs) that are both accurate and capable of realistically representing water flow are a fundamental prerequisite for hydrodynamic flood simulation. The accuracy of a DEM is critical in hydrological modelling as it can affect discharge values, water depth, and the extent of flood inundation maps (Muhadi et al., 2020).

Recent reviews of EO-based flood mapping highlight the persistent gap between two-dimensional satellite-derived flood extent products and the volumetric context provided by high-resolution three-dimensional topographic datasets, underscoring the need for hydrologically consistent DEMs as a prerequisite for physics-based flood simulation (Bates et al., 2010; Destefanis et al., 2025). However, DEMs derived from LiDAR acquisitions, as well as from imagery, are not directly suitable for hydrological modelling, as these methods capture the visible surface and therefore represent infrastructures such as bridges, tunnels and culverts as elevated terrain, artificially interrupting flow continuity even though water would normally pass beneath them (Khalid et al., 2025). In urban environments, additional sources of hydrological inconsistency include linear barriers (such as retaining walls) which might be not properly reconstructed depending on the spatial resolution or point density of the DEM. These artefacts produce spurious depressions, disconnected flow paths and unrealistic drainage patterns that propagate errors through downstream hydraulic simulations. This paper focuses on the geomatics pipeline for DEM generation and hydrological conditioning; downstream hydraulic simulation using the conditioned product will be performed separately by the Danish Meteorological Institute (DMI) and falls outside the scope of this work.

Over the years, hydrological conditioning, or the process of adjusting a DEM to better represent flow paths, has been addressed through several approaches. Classical methods include stream burning (Saunders, 1999), the AGREE surface reconditioning technique (Hellweger, 1997), outlet breaching (Martz and Garbrecht, 1999), and priority-flood depression filling (Barnes et al., 2014). These algorithmic approaches have been applied at a global scale, for instance in the HydroSHEDS dataset, to derive flow direction grids, river networks and catchment masks from SRTM elevation data (Lehner et al., 2008; Hawker et al., 2018). However, their application to high-resolution urban LiDAR DEMs requires infrastructure-specific information, such as bridge locations, culvert positions, barrier geometries, that purely elevation-based algorithms cannot infer reliably.

The integration of ancillary vector data to guide conditioning has been explored in a few recent works. GeoFabrics, an open-source Python package, provides a flexible multistage framework for assimilating elevation, natural-feature and infrastructure data, including OpenStreetMap (OSM) geometries, into hydrologically conditioned DEMs, responding to the growing need for automated and self-documenting conditioning workflows (Pearson et al., 2023). Similarly, a stepwise Python procedure has been developed to extract paved areas, water bodies and elevated road features from OSM for integration into hydraulic models, with test cases across Europe, South-East Asia and East Africa demonstrating the potential of OSM as a conditioning data source, particularly in combination with other elevation datasets (Schellekens et al., 2014). Despite these advances, existing tools present limitations in the context of high-resolution urban LiDAR DEMs: they are often designed for global or regional coarse-resolution products, rely on proprietary software components, or do not explicitly address the full range of urban infrastructure features, such as barriers, culverts and movable bridge structures, that affect drainage connectivity in dense city environments. DEMend, a recent automated correction tool, addresses bridge and culvert obstruction specifically but is designed around US-specific hydrographic datasets (NHD) and does not handle tunnel underpasses or linear barrier structures; moreover, its effectiveness depends on buffer and threshold parameters that require site-specific calibration (Khalid et al., 2025).

This paper presents an automated, open-source pipeline (written in Python language) for generating hydrologically conditioned DEMs from classified airborne LiDAR data, using OSM infrastructure geometries to drive four sequential conditioning operations: restore hydraulic connectivity beneath structures such as bridges, tunnels, and culverts, and verify the correct generation of linear barriers. The workflow is developed and tested on a 16 km² area over Copenhagen city centre, producing a 0.5 m resolution conditioned DEM for use in subsequent flood simulations. Vertical accuracy of the baseline product is assessed through independent ground control points and pixel-wise comparison against the Danish national terrain model.

2. Study Area and Data

The study area covers a 16 km² (4×4 km) portion of Copenhagen city centre, Denmark, encompassing a dense urban fabric with mixed residential and commercial land use with associated infrastructures. Copenhagen is a low-relief coastal city characterised by flat topography with elevations predominantly between 0 and 10 m above sea level (DVR90 datum), making it highly susceptible to pluvial flooding. The area includes a complex network of artificial waterways, canals, moats and harbour basins, as well as extensive road and rail infrastructure with bridges and culverts at multiple water crossings. The study area is shown in Fig. 1, along with the spatial distribution of OSM features described in 2.3.
All datasets used in this study are listed and described in the following sections. All spatial data are referenced to ETRS89 / UTM zone 32N (EPSG:25832) with vertical datum DVR90, being the native reference system for LiDAR data.

2.1 LiDAR Data

Airborne LiDAR data were acquired by the Danish Agency for Data Supply and Infrastructure (SDFE) during the 2023 national acquisition campaign. The point cloud covers the full AOI with a mean density of approximately 13.5 points/m² and comprises approximately 216 million points. Data were delivered pre-classified according to the ASPRS standard; points assigned to class 2, representing ground, were used to generate the DTM,

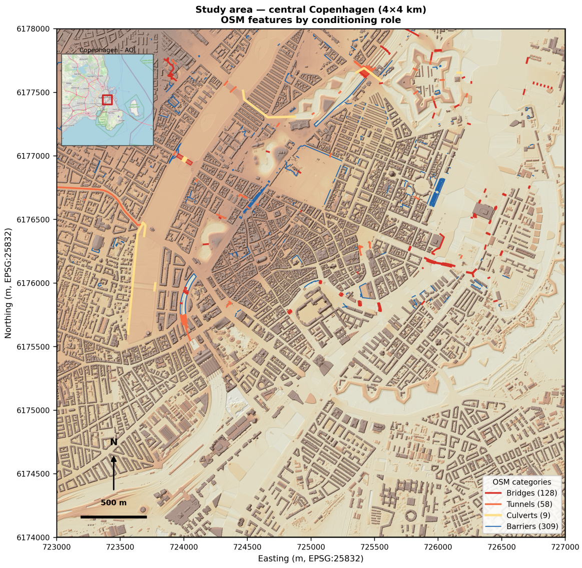

Figure 1. Study area in Copenhagen city centre (4x4 km), with OSM features extracted via Overpass API: bridges (red), tunnels (orange), culverts (yellow), and barriers (blue). Background: LiDAR-derived DTM hillshade with terrain colour overlay. Inset: overview map of eastern Denmark showing the AOI.

while points in class 6, representing buildings, were added to generate the DSM for the hydraulic modeling. No additional ground filtering was applied, as the national classification was considered sufficiently reliable for the purposes of this work. This assumption is supported by the pixel-wise validation results reported in Section 4.1 (NMAD = 0.066 m).

2.2 Reference Elevation Data

Two independent reference datasets were used for accuracy assessment. The HøjdefikspunktDanmark, a survey-grade geodetic network accessed via WFS, provided point measurements for independent validation. Benchmark selection criteria and filtering procedure are described in Section 4.1. The Danish national terrain model DHM/Terræn, maintained by SDFE and available via WCS at 0.5 m resolution (SDFE, 2023), was used for pixel-wise comparison against the LiDAR-derived DTM.

2.3 OpenStreetMap Data

Infrastructures to be removed from the DSM to enforce hydraulic connectivity (see Section 3.3) were extracted from OSM via the Overpass API. OSM has been shown to achieve sub-metre to few-metre positional accuracy in European urban areas (Haklay, 2010), and its road network exceeds 80% completeness globally, with near-complete coverage in well-governed countries with high internet penetration (Barrington-Leigh and Millard-Ball, 2017). Also, recent analyses confirm that OSM infrastructure coverage in Northern and Western European cities remains near-complete and has continued to improve over time (Herfort et al., 2023).

OSM features for the study area were downloaded using a bounding box derived from the DSM spatial extent (55.6753°N, 12.5454°E – 55.6964°N, 12.6121°E). Features were categorised into four conditioning-relevant classes following the OSM tagging conventions (OpenStreetMap Wiki, 2026): Bridges (`bridge=yes`, `bridge=movable`, `bridge=viaduct`, `bridge=aqueduct`, and `man_made=bridge`); Tunnels (`tunnel=yes`, filtered to `layer=-1` only); Culverts (`tunnel=culvert`, `waterway=culvert` and `waterway=tunnel`); and Barriers (`barrier=wall`, `barrier=retaining_wall`, `barrier=city_wall` and `barrier=coupure`).

Bridge features appear in two forms: linestrings tagged `bridge=yes` representing road or rail centrelines that cross a waterway, and polygons tagged `man_made=bridge` representing the physical bridge deck outline.

Tunnel features were filtered to retain only shallow underpasses (OSM `layer=-1`) that create artificial barriers in the LiDAR-derived DSM, where the road or terrain surface above the tunnel is captured, instead of the passage opening. Deep underground infrastructure (subway/metro at `layer` $\leq$ `-2`, typically 20–30 m below surface) was excluded as it has no expression in the surface DSM. Vertical access features (`highway=steps` and `highway=elevator`) were also excluded due to their negligible horizontal footprint and lack of hydrological relevance. Several additional OSM feature types were explicitly excluded as hydrologically irrelevant for surface conditioning: building passages, coastal structures, and natural water body polygons, whose extent is already captured in the LiDAR-derived DSM.

The final dataset comprises 505 features and constitutes the vector input to the conditioning pipeline described in Section 3.3. A summary of extracted features is provided in Table 1. Some features carry multiple OSM tags; the total reflects unique geometries.

Category	OSM tag	Count
Bridges	`bridge=yes|movable` (way)	95
Bridges	`man_made=bridge` (way/area)	34
Tunnels	`tunnel=yes, layer=-1` (way)	58
Culverts	`tunnel=culvert` (way)	9
Barriers	`barrier=wall` (way)	270
Barriers	`barrier=retaining_wall` (way)	39
Total		**505**

Table 1. OSM features extracted for the Copenhagen AOI. Each row corresponds to a distinct tag combination used for feature selection. OSM geometry types are indicated in parentheses: way (linestring or closed way), area (closed way used as polygon).

To verify the coverage of OSM elements in the study area, OSM bridge and tunnel features were cross-referenced against the GeoDanmark Bygværk dataset, the authoritative Danish register of engineered structures. Of the 186 OSM features analysed (128 bridges and 58 tunnels), 170 (91%) were matched to a corresponding reference feature, confirming near-complete coverage of conditioning-relevant infrastructure in the Copenhagen AOI and supporting the suitability of OSM as a source for DEM conditioning at 0.5 m resolution.

3. Methodology

The proposed pipeline is structured as described in the following and summarised in Figure 2: first, the classified LiDAR point cloud is rasterized to generate a DTM and a DSM, whose continuity is ensured through a combination of IDW and Natural Neighbours interpolation algorithms. Next, the relevant OSM features used to condition the elevation model are identified and extracted. Finally, the pipeline incorporates these features and applies four sequential operations to the DSM to produce a conditioned DSM, which is then used as input for flood models.

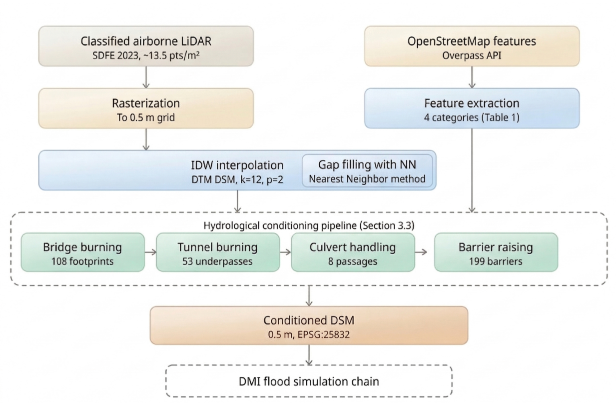

Figure 2. Workflow used to generate a conditioned DSM. Classified airborne LiDAR data are rasterized and then interpolated to produce a 0.5 m resolution DSM. OpenStreetMap features drive bridge burning, tunnel enforcing, culvert enforcing, and barrier raising. The resulting conditioned DSM is delivered for downstream flood simulation. Numbers indicate the features processed in the Copenhagen test case.

3.1 DSM and DTM Generation

A DTM and a DSM were generated from the pre-classified LiDAR point cloud: the DTM was generated using class 2 (ground), and classes 2 and 6 (ground and buildings) were combined for DSM generation. The DSM generated in this way was selected as the conditioning surface because building structures act as physical barriers that influence overland flow in urban flood simulations; their removal from the elevation surface would produce unrealistic lateral drainage through built-up blocks. The DTM, on the other hand, serves as the reference surface for bridge, tunnel and culvert conditioning operations (see Section 3.3), where DSM is burned to restore hydraulic connectivity beneath elevated infrastructure and elevations are lowered to the terrain surface where water flow occurs.

Point cloud rasterization was performed selecting the highest point within each pixel, followed by interpolation using Inverse Distance Weighting (IDW) onto a regular 0.5 m grid, producing an output raster of 8002$\times$8002 pixels in EPSG:25832. IDW was selected for its computational efficiency with dense point clouds and its well-documented suitability for flat urban terrain (Polat et al., 2015; Guo et al., 2010). Interpolation parameters were set following literature recommendations for flat urban terrain (Polat et al., 2015; Guo et al., 2010): the number of neighbours used in the interpolation was set to $k = 12$, providing a sufficient neighbourhood for stable interpolation given the points density ($\sim$13.5 pts/m^2), while limiting computational cost; the distance-decay exponent $p = 2$ is the standard IDW default, giving progressively less weight to more distant points; and the 5 m search radius ensures that gap-filled cells are flagged as NoData rather than extrapolated beyond the local point distribution.

The interpolated elevation value z was computed as:

$$z = \frac{\sum_{i=1}^{k} \frac{z_i}{d_i^p}}{\sum_{i=1}^{k} \frac{1}{d_i^p}} \tag{1}$$

where z_i and d_i are the elevation and distance of the i-th neighbour respectively, and $p = 2$ is the distance-decay exponent.

Cells for which no LiDAR points were found within the 5 m search radius were flagged as NoData in an IDW validity mask. These gaps account for approximately 22% of the output grid (ca. 14 million of 64 million cells) and are concentrated over water surfaces, where LiDAR returns are sparse or absent, and over occluded areas behind tall structures. These gaps were filled using Nearest Neighbour interpolation to ensure the spatial continuity required by the hydraulic model. Because the Nearest Neighbour algorithm propagates the elevation of the closest valid cell, the filled values over water bodies may reflect quay or embankment elevations rather than actual water surface levels. The IDW validity mask is retained as a separate layer so that downstream users (e.g., the DMI in the framework of this project) can identify gap-filled cells and apply alternative treatments where needed.

3.2 OSM Features Extraction

As already mentioned in Section 2.3, OSM features were retrieved via the Overpass API using a bounding box derived from the spatial extent of the DSM. The query targeted four conditioning-relevant categories: bridges, tunnels, culverts and barriers. Retrieved features were parsed from GeoJSON and loaded into a GeoPackage with separate layers per category using `geopandas`, and reprojected to EPSG:25832 to match the DSM coordinate reference system. Geometry types were preserved as delivered by OSM. The resulting dataset, summarised in Table 1, comprises 505 features and constitutes the primary input to the hydrological conditioning pipeline described in Section 3.3.

3.3 Hydrological Conditioning Pipeline

The hydrological conditioning pipeline modifies the DSM using OSM vector geometries through four sequential operations applied in order of hydraulic priority: bridge burning, tunnel enforcing, culvert enforcing, and barrier rasterization. Bridge, tunnel and culvert operations lower the elevation of the DSM to restore flow connectivity beneath elevated infrastructure; barrier rasterization raises the DSM to enforce the blocking effect of linear barriers not fully reconstructed in the DSM. Each operation is implemented as a raster patch, which means that only the pixels within each OSM footprint are modified, and a conservative threshold of 5 cm ($\mathrm{MIN\_LOWER} = 0.05$ m; $\mathrm{MIN\_RAISE} = 0.05$ m) prevents negligible modifications. Patch footprints and associated metadata are logged to a GeoPackage for quality control in QGIS.

Stream burning, the systematic lowering of DEM elevations along mapped waterway centrelines to enforce channel connectivity, was evaluated but not applied. In this dataset, LiDAR returns over water surfaces are classified as ASPRS class 9 and excluded from DTM interpolation, resulting in NoData cells over water bodies. These cells are subsequently filled using Nearest Neighbour interpolation, which propagates the elevation of the nearest valid cell, typically the quay or embankment edge, producing a water surface representation at approximately bankfull level. For pluvial static flood modelling this approximation is sufficient: permanent water bodies are not expected to be flood sources but must be represented as a continuous surface to avoid artefacts in flow routing and depression mapping. Stream burning would therefore introduce redundant and potentially erroneous modifications to a surface already correctly handled by the gap-filling step. This decision is specific to datasets where water returns are pre-classified and may not generalize to LiDAR acquisitions without class 9 labeling.

3.3.1 Bridge Burning The first step in the conditioning process to enforce hydraulic connectivity is bridge burning. Because DEMs represent the upper surface of the terrain, they cannot capture the voids beneath elevated structures. Consequently, passages that allow water to flow underneath or through them are not represented, which leads to incorrect drainage paths in hydrological analyses. Bridge burning replaces DSM elevation within each bridge footprint with the corresponding DTM elevation, restoring hydraulic connectivity.

Bridge footprints were constructed from two OSM source types. For features tagged `man_made=bridge` (34 polygon geometries), the OSM outline was used directly as the footprint. For features tagged `bridge=yes` or `bridge=movable` (95 linestring geometries representing road and rail centrelines), a transverse buffer was applied to approximate the deck width. For both bridge and tunnel linestrings, the buffer width was set to the value of the OSM `width=` tag when present, or estimated from the `lanes=` tag (4.0 m per lane); where neither tag was available, a default total width of 12 m was applied, corresponding to a 6 m buffer on each side of the centreline. The same width estimation hierarchy was applied to tunnel features, as tunnel width corresponds to the carriageway passing through the structure. The default value of 12 m is consistent with standard two-lane road dimensions in European design practice (AASHTO, 2018). This reliance on a single default value is a recognised limitation: Copenhagen's infrastructure includes narrow pedestrian tunnels (2–3 m) as well as wide rail underpasses (>20 m), for which the 12 m default may respectively over- or under-estimate the footprint.

To avoid erroneously lowering building pixels adjacent to bridge or tunnel footprints, a building mask was applied. Pixels where the normalised DSM (nDSM = DSM − DTM) exceeded 3.0 m were excluded from patching. The 3.0 m threshold was chosen as a conservative discriminator between bridge deck / tunnel road surfaces and adjacent building volumes; it is consistent with minimum building height assumptions; however, this value may require adjustment in cities with different building typologies. The building mask (nDSM > 3.0 m) mitigates over-buffering artefacts. For each bridge footprint, DSM pixels were replaced with the corresponding DTM elevation, restoring the terrain surface beneath the structure.

3.3.2 Tunnel and Culvert Enforcement Tunnel footprints were constructed from 58 linestring features tagged `tunnel=yes` at OSM `layer=-1`, representing shallow underpasses for roads, railways, cycleways and pedestrian paths. The same elevation-replacement logic as bridge burning was applied: DSM pixels within each tunnel footprint were replaced with the corresponding DTM elevation, restoring the surface level that would be observed at the tunnel portal rather than the road surface above. The same buffer width estimation hierarchy described in Section 3.3.1 was applied to determine footprint width.

Culverts are subsurface waterway passages beneath roads or embankments. In the LiDAR-derived DSM, the road surface above

https://doi.org/10.5194/isprs-archives-XLIX-B2-2026-151-2026

a culvert is recorded at road grade, interrupting the modelled waterway at the crossing point. Culvert handling applies the same elevation-replacement logic: pixels within the culvert footprint are assigned the DTM elevation to open a hydraulic passage. Footprints for the nine OSM culvert features (`tunnel=culvert`) were generated by buffering each node or linestring geometry by 3 m, producing circular or rectangular footprints centred on the culvert location.

3.3.3 Barrier Rasterization Flood defence barriers, retaining walls, sea walls and city walls, may be underrepresented in the LiDAR-derived DSM if their narrow cross-section is captured by few points, or if classification wrongly assigns wall-top returns to ground points (class 2). Barrier rasterization raises DSM pixels along OSM barrier geometries to the measured top-of-wall elevation, ensuring that barriers function as continuous blocking elements in hydraulic simulations. Since top-of-wall elevations are not available as OSM attributes, they were derived from the LiDAR point cloud. For each barrier geometry (`wall`, `retaining_wall`, `city_wall`; $n = 309$), a 0.6 m-wide horizontal buffer (0.3 m on each side of the centerline) was applied and all non-ground, non-building, non-noise points within the buffer (excluding points assigned to ASPRS classes 2, 6, 7 and 18) were extracted. A wider buffer (e.g., 0.5 m) would increase point capture but risk sampling off-wall returns; the 0.3 m value was chosen conservatively to minimise this contamination. The 90th percentile of the resulting point elevations was taken as the top-of-wall height. To ensure vertical reliability, a barrier was processed only if at least three LiDAR points were identified within this narrow strip. Given the mean inter-point spacing of $\sim$0.27 m, this three-point threshold acts as a rigorous quality filter, requiring consistent returns along the barrier's crest rather than isolated noise. The sensitivity of the exclusion rate to buffer width was not formally tested; a systematic comparison of buffer values (0.3, 0.5, 1.0 m) against manually measured wall heights is recommended for future implementations.

Out of 309 barriers, 201 met the reliability criterion and additionally satisfied the plausibility filter (height above ground $\in [0, 10]$ m); the remaining 108 features were intentionally excluded due to insufficient LiDAR density within the 0.6 m buffer. This conservative approach avoids introducing elevation artefacts in areas of sparse point coverage. For each barrier that met the criteria, the geometry was buffered by 0.3 m to ensure raster coverage on the 0.5 m grid, and the footprint was rasterized onto the DSM. Pixels within the footprint were raised to $z_{\mathrm{lidar,top}}$ only if $z_{\mathrm{lidar,top}}$ exceeded the current DSM value by more than 0.05 m; no pixel was lowered. Out of 201 candidate barriers, 199 produced at least one raised pixel. The full methodology is shown in Figure 2.

4. Accuracy Assessment

4.1 Checkpoint Validation against HøjdefikspunktDanmark

Independent validation was performed using survey grade points from the HøjdefikspunktDanmark network, accessed via WFS. An initial candidate set of 562 points fell within the AOI. However, the dataset presented a fundamental compatibility issue: most Danish survey grade benchmarks are affixed to vertical surfaces of permanent structures such as building facades, bridge abutments, retaining walls, and therefore carry elevations representative of structural attachment points rather than bare-earth terrain. Validating the DTM against such benchmarks introduces a systematic incompatibility that cannot be resolved by coordinate-based filtering alone. Candidates were filtered according to three criteria: benchmark type restricted to ground-level installations, internal precision (*middelfejl*) $\leq$ 15 mm, and location within IDW-valid DTM cells. After filtering, 37 benchmarks were retained, representing 7% of the initial candidate set. The high rejection rate (88%) reflects the structural composition of the network rather than a limitation of the DTM and constitutes itself a finding regarding the practical usability of HøjdefikspunktDanmark for LiDAR product validation in dense urban environments.

The generated DTM was validated against the aforementioned survey-grade control points, yielding the metrics presented in Table 2. A pixel-wise comparison against the national DHM/Terræn, constituting the primary accuracy assessment, is presented in the following section. The DSM was then generated by adding building points (ASPRS class 6) to the ground class, as described in Section 3.1.

Metric	**Pixel-wise DHM/Terræn**	**Survey Højdefiks.**
n	$\sim$50M pixels	37 points
Bias (m)	-0.018	-0.568
SD (m)	0.611	0.393
NMAD (m)	0.066	0.244
RMSE (m)	0.611	0.691
LE90 (m)	0.265	–
LE95 (m)	0.547	–

Table 2. Vertical accuracy assessment of the LiDAR-derived DTM against DHM/Terræn (pixel-wise) and HøjdefikspunktDanmark survey grade points (checkpoint validation).

Results for the filtered subset show a systematic bias of -0.568 m and an NMAD of 0.244 m. The bias is interpreted as a residual effect of the filtering procedure: even among benchmarks classified as ground-level, a proportion are installed on elevated horizontal surfaces such as kerb stones, steps or plinths, which remain above the bare-earth interpolation surface. Once the systematic offset is accounted for, the random component of the discrepancy is consistent with the expected accuracy of the DTM in areas affected by local microtopographic complexity. It is acknowledged that this interpretation cannot fully exclude a contribution from genuine DTM error at benchmark locations, particularly in areas of local microtopographic complexity. The bias likely reflects a combination of residual benchmark installation height and genuine DTM error at structurally complex locations; the two contributions cannot be separated with the available data.

The pixel-wise comparison against DHM/Terræn, which shares the same bare-earth definition and spatial resolution as the LiDAR-derived product, is therefore considered the primary accuracy assessment for this study. Figure 3 shows the spatial distribution of vertical errors over a 1.5×1.5 km subset and the error frequency distribution computed over the full 4×4 km AOI (IDW-valid pixels only).

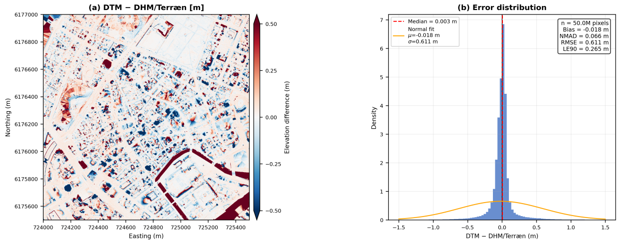

Figure 3. Vertical accuracy of the LiDAR-derived DTM against DHM/Terræn. (a) Pixel-wise difference map (1.5×1.5 km subset); diverging colormap clipped at ±0.5 m. (b) Error frequency distribution and statistics computed over the full 4×4 km AOI (IDW-valid pixels only).

4.2 Pixel-wise Validation against DHM/Terræn

The LiDAR-derived DTM was also validated by pixel-wise comparison against the official Danish DTM, resampled to the same 0.5 m grid via bilinear interpolation. The comparison was restricted to IDW-valid cells, yielding approximately 50-million-pixel pairs. Vertical accuracy was quantified using bias, RMSE, the Normalised Median Absolute Deviation (NMAD) and linear error at the 90th and 95th percentiles (LE90, LE95). NMAD and sample quantiles were adopted as primary accuracy measures following Höhle and Höhle (2009) and Aguilar et al. (2010), who demonstrate that LiDAR-derived DEMs frequently exhibit non-Gaussian error distributions due to imperfect filtering at vegetation and building edges, making RMSE an unreliable estimator in such conditions. The pixel-wise SD of 0.611 m nearly equals the RMSE because the bias is negligible (-0.018 m); however, the SD/NMAD ratio of $\sim$9$\times$ indicates heavy-tailed residuals driven by $\sim$5% outliers at vegetation and building edges, confirming that NMAD is the representative accuracy metric for this dataset. In contrast, the checkpoint SD of 0.393 m yields a SD/NMAD ratio of $\sim$1.6$\times$, closer to a Gaussian distribution, indicating that the large checkpoint RMSE (0.691 m) is dominated by the systematic bias (-0.568 m) rather than by random scatter.

The NMAD of 0.066 m indicates strong agreement with the reference surface for most valid cells, consistent with the 6 cm RMSE accuracy declared by SDFE for DHM/Terræn. The bias of -0.018 m is negligible. The RMSE of 0.611 m substantially exceeds the NMAD, consistent with the presence of residual outliers ($\sim$5% of valid cells) at class boundaries where ground classification is imperfect.

5. Results and Discussion

5.1 Bridge, Tunnel and Culvert Burning and Barrier Rasterization

From the 505 OSM features, 195 bridge, tunnel and culvert footprints were constructed: 34 bridge polygons used directly, 95 bridge linestrings buffered to a transverse width (default 12 m), 58 tunnel linestrings buffered using the same width estimation hierarchy, and 9 culverts buffered to a 3 m radius. Of these, 169 footprints resulted in at least one DSM pixel being lowered; the remaining 26 were skipped: 10 because the DSM was already at or below the DTM elevation within the footprint, and the remainder due to empty geometry or location outside the valid raster extent. The building mask (nDSM threshold 3.0 m) prevented modification of footprints where bridge or tunnel line buffers overlapped adjacent structures.

By feature type, 79 bridge linestrings, 29 bridge polygons, 53 tunnels, and 8 culverts produced modified pixels, for a total of 198,733 lowered pixels with a median elevation reduction of 0.69 m and a maximum of 10.08 m. The addition of tunnel features alone contributed 53 conditioned footprints and approximately 53,000 lowered pixels, representing a substantial component of the total hydraulic connectivity restoration.

The bridge burning and tunnel and culvert enforcement step is methodologically analogous to the set of hydrological corrections distributed by SDFE alongside the Danish national DHM/Terræn, which encode manual elevation adjustments at bridge openings and culvert passages to restore hydraulic connectivity. Producing these corrections is a labour-intensive process largely performed manually (Arge and Grønlund, 2019). That our OSM-driven pipeline independently recovers a comparable set of hydraulic openings constitutes a qualitative validation of the approach. Quantitative comparison of the two conditioning datasets is identified as a priority for future work, as it would allow the completeness and positional accuracy of OSM-driven conditioning to be benchmarked against an authoritative national reference.

Regarding barrier rasterization, out of 309 OSM barrier features (270 `barrier=wall`, 39 `barrier=retaining_wall`), 201 satisfied the reliability criteria (minimum 3 LiDAR returns within a 0.3 m buffer, height above ground $\in [0, 10]$ m); no `city_wall` or `coupure` features were present in the AOI. The remaining 108 features (35%) lacked sufficient point density within the narrow buffer and were excluded, constituting a recognised limitation of the LiDAR-based top-of-wall height estimation. Among the 201 reliable barriers, 199 produced raised pixels (2 were already above their measured top-of-wall height). A total of 27,022 DSM pixels were raised, with a median measured height above ground of 3.00 m (10th–90th percentile range: 0.96–8.22 m) and a median DSM elevation increase of 4.53 m, consistent with the heights expected for Copenhagen's harbour walls and canal retaining structures. Figure 4 shows an example of a retaining wall rasterised with this approach, where the LiDAR-derived top-of-wall height is $h = 5.7$ m above ground ($z_{\mathrm{top}} - \mathrm{DTM}$), corresponding to an absolute elevation of $z_{\mathrm{top}} = 8.1$ m (DVR90).This correction is equivalent to adjusting the initial DSM elevation from an underestimated value of 2.4 m to the validated elevation of 8.1 m, effectively recovering the 5.7 m vertical offset through the rasterization process.

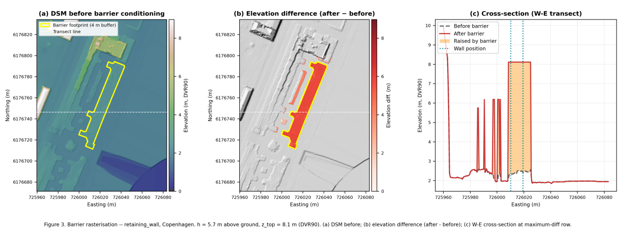

Figure 4. Barrier rasterization at a retaining wall, Copenhagen. (a) DSM before conditioning; (b) elevation difference (after minus before); (c) W–E cross-section at the row of maximum elevation difference. Dashed grey line: original DSM; solid red line: conditioned DSM;dashed cyan line: wall position.

5.2 Conditioning Effect Quantification

The hydrological conditioning pipeline modifies the DSM through targeted elevation patches applied at bridge, tunnel, culvert, and barrier locations. To quantify the cumulative effect of these modifications at the DEM level, a global depression analysis was performed using `pysheds` priority-flood filling on both the unconditioned and conditioned DSM. The total trapped depression volume decreased from 14.50 Mm^3 to 13.78 Mm^3 ($-718{,}496$ m^3, -5.0%), corresponding to a reduction in depressed area of 0.20 km^2. The residual depression volume is dominated by legitimate topographic features (canals, harbour basins, sunken road segments) and does not represent artefacts. No closed depressions with no outlet (D8 sinks, i.e. cells from which all eight neighbouring cells are at higher elevation) were identified in either DSM, consistent with Copenhagen's flat coastal topography where all flow paths drain to the AOI boundary. The addition of tunnel features alone contributed roughly half of the total depression reduction: without tunnel conditioning, the reduction would have been approximately $-325{,}000$ m^3 (-2.2%), confirming that shallow underpasses are a quantitatively significant source of artificial impoundment in dense urban DSMs. These metrics quantify the geomatics conditioning effect, that is how much the elevation surface changed, and should not be interpreted as hydraulic model validation.

The usability of the conditioned DSM for flood simulation is subject to the following constraints. First, the pixel-wise RMSE of 0.611 m, while dominated by outliers at class boundaries, reflects residual elevation uncertainty that may influence depth estimates in low-relief terrain where flood depths are of comparable magnitude; the NMAD of 0.066 m is the representative accuracy for the majority of the surface. Second, the conditioning addresses only the features captured in OSM at the time of extraction; structures absent from OSM are not corrected. These limitations are inherited by any downstream hydraulic simulation and should be explicitly acknowledged by the model operator. Full event-based hydraulic validation falls outside the scope of this work and will be performed separately.

Several terrain and hydrological processes were deliberately excluded from the conditioning pipeline as they fall outside the scope of DSM preparation and are handled by the downstream hydraulic model. Vegetation returns (ASPRS classes 3–5) are excluded from DSM generation: trees and shrubs do not constitute geometric obstacles in a static hydraulic model, and their effects on rainfall interception, surface roughness and flow retardation are parameterised within the model itself. Soil permeability and infiltration capacity are not encoded in the DSM but are represented through land-use-dependent parameters in the flood simulation chain. Subsurface storage volumes such as underground car parks and building basements are not accounted for, a conservative assumption that may lead to overestimation of inundation extent, preferable to underestimation in a risk management context. Finally, depression filling and sink resolution are not performed in this paper: residual depressions are passed to the hydraulic model, which applies its own treatment.

6. Conclusions

This paper presented an automated, open-source Python pipeline for generating hydrologically conditioned DEMs from classified airborne LiDAR data and OpenStreetMap infrastructure geometries. The workflow was developed and validated on a 16 km^2 portion of central Copenhagen using a 2023 national LiDAR acquisition at 13.5 pts/m^2, producing a 0.5 m resolution conditioned DSM for subsequent use in urban flood simulations.

The baseline DTM achieved NMAD $= 0.066$ m against the Danish national reference DHM/Terræn, confirming that IDW interpolation of pre-classified LiDAR at this density yields a product of high intrinsic accuracy. Hydrological conditioning was performed through four sequential operations driven exclusively by OSM vector geometries: bridge burning restored hydraulic connectivity at 108 crossing footprints (79 linestring, 29 polygon), tunnel enforcing opened 53 shallow underpasses, culvert enforcing opened 8 subsurface passages, and barrier rasterization raised 199 flood defence structures to their LiDAR-measured top-of-wall elevations. In total, 198,733 pixels were lowered with a median elevation correction of 0.69 m, and 27,022 pixels were raised with a median height of 3.00 m above ground. The combined conditioning reduced the trapped depression volume in the DSM by 718,496 m^3 (-5.0%). The bridge burning, and tunnel and culvert enforcement results, were independently corroborated by their structural similarity to the DHM Tilpasningslag layers (the official set of hydrological corrections to the Danish national terrain model), embedded in the national DHM/Terræn product.
The inclusion of tunnel features (`tunnel=yes` at OSM `layer=-1`) proved to be a significant addition to the conditioning pipeline: the 53 tunnel footprints contributed approximately one third of the total lowered pixels and more than doubled the trapped volume reduction compared to bridge and culvert conditioning alone (-718k m^3 vs -325k m^3 without tunnels). This finding highlights the importance of including shallow underpasses, and not only bridges and culverts, in DEM hydrological conditioning workflows for dense urban environments.

The pipeline is fully scripted, modular and parameterised, requiring only pre-classified LiDAR data and an internet connection to download OSM geometries from the Overpass API. Its dependence on OSM completeness is the primary transferability constraint: mapping of bridge, tunnel, culvert and barrier geometries is high in European cities but may be incomplete in less-mapped regions (Barrington-Leigh and Millard-Ball, 2017).

Few limitations of the present implementation should be noted. First, the assessment of hydrological impact is limited to metrics derived from the storage volume of topographic depressions identified in the DEM. The analysis therefore provides a static, terrain-based representation of flooding, evaluating potential flow paths and areas where water can accumulate. Event-based hydraulic validation is deferred to the operational simulation chain. Second, the default 12-meter buffer for bridge and tunnel lines has not undergone sensitivity analysis and may require site-specific calibration in cities with different infrastructure types. Third, the tunnel filtering strategy (`layer=-1`, which excludes subway features and vertical accesses) relies on the quality and completeness of OSM tagging, which may vary in less well-mapped regions. These limitations define the boundary conditions for the transferability of the pipeline to other European urban contexts.

Three further directions for future work are identified: (i) quantitative benchmarking of OSM-driven bridge, tunnel and culvert conditioning against the Danish DHM Tilpasningslag to establish completeness and positional accuracy metrics transferable to other national contexts; (ii) sensitivity analysis of the buffer width parameter across cities with varying infrastructure typologies; and (iii) application of the pipeline to additional European urban centres, where pre-classified national LiDAR and OSM infrastructure coverage are comparably mature, and accurate ground points for DEM validation are available, to evaluate the transferability of the methodology.

The pipeline will be made publicly available upon publication to support reproducible hydrological DEM conditioning in urban flood modelling workflows.

Acknowledgements

This work was carried out within the CLEAR-EO project, funded by the European Union under the Horizon Europe programme (Grant Agreement No. 101182722). The authors acknowledge Klimadatastyrelsen (The Danish Agency for Climate Data) for providing the DHM/Punktsky open Lidar dataset used in this study.

References

Aguilar, F.J., Mills, J.P., Delgado, J., Aguilar, M.A., Negreiros, J.G., Pérez, J.L., 2010. Modelling vertical error in LiDAR-derived digital elevation models. *ISPRS Journal of Photogrammetry and Remote Sensing*, 65(1), 103–110. DOI: 10.1016/j.isprsjprs.2009.09.003

Arge, L., Grønlund, A., 2019. Learning to Find Hydrological Corrections. arXiv:1909.07685

Arnbjerg-Nielsen, K., Willems, P., Olsson, J., Beecham, S., Pathirana, A., Bülow Gregersen, I., Madsen, H., Nguyen, V-T-V., 2013. Impacts of climate change on rainfall extremes and urban drainage systems: a review. *Water Science and Technology*, 68(1), 16–28. DOI: 10.2166/wst.2013.251

AASHTO, 2018. *A Policy on Geometric Design of Highways and Streets*, 7th Edition. American Association of State Highway and Transportation Officials, Washington, D.C.

Barnes, R. et al., 2014. Priority-flood: An optimal depression-filling and watershed-labeling algorithm for digital elevation models. *Computers & Geosciences*, 62, 117–127. DOI: 10.1016/j.cageo.2013.04.024

Barrington-Leigh, C., Millard-Ball, A., 2017. The world's user-generated road map is more than 80% complete. *PLoS ONE*, 12(8), e0180698. DOI: 10.1371/journal.pone.0180698

Bates, P.D., Horritt, M.S., Fewtrell, T.J., 2010. A simple inertial formulation of the shallow water equations for efficient two-dimensional flood inundation modelling. *Journal of Hydrology*, 387(1–2), 33–45. DOI: 10.1016/j.jhydrol.2010.03.027

City of Copenhagen, 2012. *Cloudburst Management Plan*. Technical and Environmental Administration, Copenhagen Municipality. Available at: `https://international.kk.dk/sites/default/files/2021-09/Cloudburst\%20Management\%20plan\%202010.pdf`

Destefanis, T., Guliyeva, S., Boccardo, P., Fissore, V., 2025. Advancing Flood Detection and Mapping: A Review of Earth Observation Services, 3D Data Integration, and AI-Based Techniques. *Remote Sensing*, 17(17), 2943. DOI: 10.3390/rs17172943

Guo, Q. et al., 2010. Effects of topographic variability and lidar sampling density on several DEM interpolation methods. *Photogrammetric Engineering and Remote Sensing*, 76(6), 701–712. DOI: 10.14358/PERS.76.6.701

Haklay, M., 2010. How good is volunteered geographical information? A comparative study of OpenStreetMap and Ordnance Survey datasets. *Environment and Planning B: Planning and Design*, 37(4), 682–703. DOI: 10.1068/b35097

Hawker, L. et al., 2018. Perspectives on Digital Elevation Model (DEM) Simulation for Flood Modeling in the Absence of a High-Accuracy Open Access Global DEM. *Frontiers in Earth Science*, 6, 233. DOI: 10.3389/feart.2018.00233

Hellweger, F., 1997. AGREE – DEM Surface Reconditioning System. University of Texas at Austin.

Herfort, B., Lautenbach, S., Porto de Albuquerque, J., Anderson, J., Zipf, A., 2023. A spatio-temporal analysis investigating completeness and inequalities of global urban building data in OpenStreetMap. *Nature Communications*, 14, 3985. DOI: 10.1038/s41467-023-39698-6

Höhle, J., Höhle, M., 2009. Accuracy assessment of digital elevation models by means of robust statistical methods. *ISPRS Journal of Photogrammetry and Remote Sensing*, 64(4), 398–406. DOI: 10.1016/j.isprsjprs.2009.02.003

IPCC, 2022. *Climate Change 2022: Impacts, Adaptation and Vulnerability*. Cambridge University Press. DOI: 10.1017/9781009325844

Khalid, Z., de Souza de Lima, A., Ruess, P.J., Khalid, A., Miesse, T., Veronez, D., Ferreira, C.M., Kinter, J.L., 2025. DEMend: Automating Hydrological Correction of Digital Elevation Models for Enhanced Urban Flood Modeling. *Water Resources Management*, 39, 5751–5768. DOI: 10.1007/s11269-025-04226-2

Lehner, B., Verdin, K., Jarvis, A., 2008. New global hydrography derived from spaceborne elevation data. *Eos, Transactions, AGU*, 89(10), 93–94.

Martz, L.W., Garbrecht, J., 1999. An outlet breaching algorithm for the treatment of closed depressions in a raster DEM. *Computers & Geosciences*, 25(7), 835–844.

Muhadi, N.A., Abdullah, A.F., Bejo, S.K., Mahadi, M.R., Mijic, A., 2020. The Use of LiDAR-Derived DEM in Flood Applications: A Review. *Remote Sensing*, 12(14), 2308. DOI: 10.3390/rs12142308

OpenStreetMap Wiki, Key:layer. `https://wiki.openstreetmap.org/wiki/Key:layer` (accessed March 2026).

Pearson, R.A., Smart, G., Wilkins, M., Lane, E.M., Harang, A., Bosserelle, C., Cattoën, C., Measures, R., 2023. GeoFabrics 1.0.0: An open-source Python package for automatic hydrological conditioning of digital elevation models for flood modelling. *Environmental Modelling & Software*, 170, 105842. DOI: 10.1016/j.envsoft.2023.105842

Polat, N., Uysal, M., Toprak, A.S., 2015. An investigation of DEM generation process based on LiDAR data filtering, decimation, and interpolation methods for an urban area. *Measurement*, 75, 50–56. DOI: 10.1016/j.measurement.2015.08.008

Saunders, W., 1999. Preparation of DEMs for use in Environmental Modelling Analysis. *ESRI User Conference Proceedings*.

Schellekens, J., Brolsma, R.J., Dahm, R.J., Donchyts, G.V., Winsemius, H.C., 2014. Rapid setup of hydrological and hydraulic models using OpenStreetMap and the SRTM derived digital elevation model. *Environmental Modelling & Software*, 61, 98–105. DOI: 10.1016/j.envsoft.2014.07.006

SDFE, 2023. Danmarks Højdemodel – DHM/Terræn. Danish Agency for Data Supply and Infrastructure. Available at: `https://datafordeler.dk`